Silver Nanoparticles Decorated Reduced Graphene Oxide (rGO) Nanosheet: A Platform for SERS Based Low-level Detection of Uranyl Ion.

ARTICLE *in* ACS APPLIED MATERIALS & INTERFACES · AUGUST 2013

Impact Factor: 6.72 · DOI: 10.1021/am4025017 · Source: PubMed

6 AUTHORS, INCLUDING:

Soumen Dutta
IIT Kharagpur
22 PUBLICATIONS **125** CITATIONS
SEE PROFILE

Mukul Pradhan
Pohang University of Science and Technology
45 PUBLICATIONS **757** CITATIONS
SEE PROFILE

Yuichi Negishi
Tokyo University of Science
89 PUBLICATIONS **4,455** CITATIONS
SEE PROFILE

Tarasankar Pal
IIT Kharagpur
255 PUBLICATIONS **8,754** CITATIONS
SEE PROFILE

ACS APPLIED MATERIALS & INTERFACES

Research Article

www.acsami.org

Silver Nanoparticle Decorated Reduced Graphene Oxide (rGO) Nanosheet: A Platform for SERS Based Low-Level Detection of Uranyl Ion

Soumen Dutta,[†] Chaiti Ray,[†] Sougata Sarkar,[†] Mukul Pradhan,[†] Yuichi Negishi,[‡] and Tarasankar Pal*[,†]

[†]Department of Chemistry, Indian Institute of Technology, Kharagpur 721302, India

[‡]Department of Applied Chemistry, Tokyo University of Science, Tokyo 1628601, Japan

Supporting Information

ABSTRACT: Herein, a simple wet-chemical pathway has been demonstrated for the synthesis of silver nanoparticle conjugated reduced graphene oxide nanosheets where dimethylformamide (DMF) is judiciously employed as an efficient reducing agent. Altogether, DMF reduces both silver nitrate ($AgNO_3$) and graphene oxide (GO) in the reaction mixture. Additionally, the presence of polyvinylpyrolidone (PVP) assists the nanophasic growth and homogeneous distribution of the plasmonic nanoparticle Ag(0). Reduction of graphene oxide and the presence of aggregated Ag NPs on reduced graphene oxide (rGO) nanosheets are confirmed from various spectroscopic techniques. Finally, the composite material has been exploited as an intriguing platform for surface enhanced Raman scattering (SERS) based selective detection of uranyl (UO_2^{2+}) ion. The limit of detection has been achieved to be as low as 10 nM. Here the normal Raman spectral (NRS) band of uranyl acetate (UAc) at 838 cm^{-1} shifts to 714 and 730 cm^{-1} as SERS bands for pH 5.0 and 12.0, respectively. This distinguished Raman shift of the symmetric stretching mode for UO_2^{2+} ion is indicative of pronounced charge transfer (CT) effect. This CT effect even supports the higher sensitivity of the protocol toward UO_2^{2+} over other tested oxo-ions. It is anticipated that rGO nanosheets furnish a convenient compartment to favor the interaction between Ag NPs and UO_2^{2+} ion through proximity induced adsorption even at low concentration.

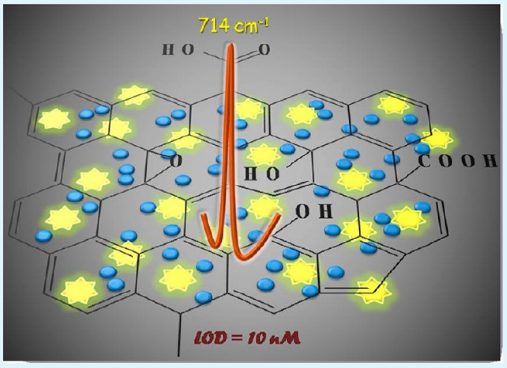

KEYWORDS: *Reduced graphene oxide, plasmonic nanoparticle, uranyl ion, charge transfer, limit of detection*

INTRODUCTION

Graphene stands to be a promising 2D-carbon lattice in the field of material research due to its excellent chemical and physical properties.[1] Large surface area, unique thermal and chemical stability, excellent mechanical strength, and superior electrical conductivity make graphene a potential component in various fields such as solar cells,[2] energy storage device,[3] sensors,[4] energy conversion,[5] and so forth. A chemically available source of graphene is graphite which needs to be exfoliated into free aromatic sheets of sp^2-bonded carbon atoms. But due to its highly hydrophobic nature, aqueous solution based approaches proceed through graphene oxide (GO) which is composed of functionalized graphene-like sheets. The hydroxyl, carboxyl, and epoxide groups in GO stabilize the aqueous dispersion of GO.[6] Recently, enormous interests have been drawn for the development of graphene based hybrid materials where semiconductors, metal nanoparticles (Au, Pd, Pt, etc.), conducting polymers exhibit higher performance in their respective applications with the assistance of graphene in the nanocomposite systems.[7]

Since the discovery of surface enhanced Raman scattering (SERS) from a silver surface,[8] a renewed importance has been created for the interpretation of enhanced vibrational nature of an adsorbate on a rough surface. Hence, SERS becomes a powerful analytical tool in various fields of research such as sensing, catalysis, explosive detection, and so forth.[9] Ultrahigh sensitivity of SERS opens up a new avenue for single molecule detection of a probe molecule in recent years.[10] Raman enhancement originates from two distinct phenomena: long-range electromagnetic effect (EM) and short-range chemical effect (CE).[9] Localized surface plasmon resonance (LSPR) from metal nanoparticle (NP) provides a suitable surface for superior Raman scattering studies. Since the EM effect is more prominent for SERS, the coinage metal NPs, especially silver and gold, are the most desirable candidates for designing SERS substrate[9] although transition metal NPs have the capability but in limited cases.[11]

Recently, graphene has become a new class of SERS substrate for efficient Raman scattering of a molecule adsorbed on the graphene surface. The idea behind this phenomenon can be explained considering charge transfer (CT) from graphene to the adsorbate,[12] resulting in the enhancement of SERS signal

Received: June 27, 2013
Accepted: August 15, 2013
Published: August 15, 2013

   dx.doi.org/10.1021/am4025017 | ACS Appl. Mater. Interfaces 2013, 5, 8724−8732

intensity which is basically known as chemical enhancement (CE). Fluorescence background interferes with the Raman signal which causes a huge problem to obtain the signature of a fluorescent molecule by resonance Raman spectroscopy (RRS). Graphene, being a known fluorescence quencher, leaves a promise and becomes an effective SERS substrate for fluorescent molecules.[13] Since the CT phenomenon is distance dependent, the adsorption of a molecule onto graphene sheet plays a major role in this case. The graphene surface can be modified by various processes for useful applications. Graphene oxide (GO) or its reduced form consists of some defects in terms of functionalization by some oxygen containing groups. To show the dominance of CE, Yu et al. described SERS of Rhodamine B (RhB) deploying rGO which was obtained in successive stages after different degrees of reduction.[14] Here oxygen containing groups of rGO direct the interactions between substrate and RhB. The large surface area of graphene or graphene derivatives and their functional groups support efficient adsorption of various organic molecules[15] and ions[16,17] through $\pi-\pi$ stacking and electrostatic interactions, respectively. This capability produces a semiconductor with improved photocatalytic activity when it gets hybridized with rGO.[18] Inspired by the enhanced SERS activity of silver,[19] nowadays synthesis of Ag NPs deposited GO or rGO sheets is going to be highly demanding for SERS measurement where pronounced charge transfer excitation can be coupled with strong electromagnetic effects.[20] Then potential SERS substrates by incorporating Ag NPs in GO or rGO provide new platforms with improved SERS effect for various well-known Raman reporters.[21−27] In most of the cases, $\pi-\pi$ interaction, electrostatic interaction, and adsorption are proposed to be the major factors to acquire an improved SERS spectrum.[21,26,27] Recently, GO or rGO conjugated noble metal nanoparticles have been reported as an effective SERS substrate for selective pesticide[28] and explosive[29] detection.

Uranium is an essential component in nuclear fuel and it is generally found as uranyl (UO_2^{2+}) ion in various salts. This ion sometimes contaminates groundwater as spent nuclear fuel is sometimes disposed into water. Though the chemical behavior of U(VI) as UO_2^{2+} in aqueous medium is well-known through several studies,[30,31] trace detection of this ion is necessary due to its huge environmental concern. The symmetric stretching mode of oxo-bridged UO_2^{2+} appears around 850 cm^{-1} in normal a Raman spectrum (NRS). Several approaches were followed to study the Raman spectrum of UO_2^{2+} ion when it is adsorbed onto differently modified or unmodified metal surfaces.[32−38] Sepaniak et al. observed the appearance of a broad band for symmetric stretching of UO_2^{2+} ion around 700 cm^{-1} on a thermally vapor deposited silver surface.[39] This large shift was explained in terms of the CT from silver to UO_2^{2+} ion. The band position for symmetric stretching (ν_1) mode of uranyl species highly depends on experimental conditions such as nature of metal surfaces, temperature, pH of solution, and so forth[34,36,39] which strongly suggest that the adsorption mechanism of UO_2^{2+} ion on SERS substrate is very important. Herein, we are disclosing that graphene nanocomposite becomes an excellent substrate for trace UO_2^{2+} detection when silver nanoparticles are immobilized properly on the surface of rGO sheets. To the best of our knowledge, this is the first report where silver nanoparticle decorated reduced graphene oxide (Ag-rGO) sheets have been employed as an efficient SERS substrate for detection of the uranyl ion.

EXPERIMENTAL SECTION

Materials. All the reagents used were of AR grade and used as received without further purification. Graphite powder, uranyl acetate (UAc), and uranyl nitrate (UN) were purchased from Sigma-Aldrich. Potassium permanganate, sodium nitrate, hydrogen peroxide, sulfuric acid, hydrochloric acid, silver nitrate, PVP (K-30), *N*,*N*-dimethylformamide (DMF), sodium hydroxide, and ethanol were purchased from Merck, India. Sodium borohydride ($NaBH_4$), sodium hydrogen arsenate ($Na_2HAsO_4{\cdot}7H_2O$), potassium chromate (K_2CrO_4), sodium molybdate ($Na_2MoO_4{\cdot}2H_2O$), vanadyl sulfate ($VOSO_4{\cdot}5H_2O$), and sodium tungstate ($Na_2WO_4{\cdot}2H_2O$) were purchased from SRL, India. All glassware were cleaned using aqua-regia, subsequently rinsed with a copious amount of double distilled water, and dried well prior to use. Double distilled water was used throughout the course of the investigation.

Instrumentation. FESEM analysis was done with a supra, Carl Zeiss Pvt. Ltd. Instrument and compositional analysis of the sample was completed with an energy dispersive X-ray microanalyzer (OXFORD ISI 300 EDAX) attached to the scanning electron microscope. Transmission electron microscopic (TEM) analyses of the samples were carried out on a Hitachi H-9000 NAR transmission electron microscope, operating at 100 kV. XRD was recorded on a Philips PW-1710 X-ray diffractrometer (40 kV, 20 mA) with Cu Kα radiation (λ = 1.5418 Å) in the 2θ range of 5°−80° at a scanning rate of 0.5° min^{-1}. Fourier transform infrared (FTIR) studies were performed with a Thermo-Nicolet continuum FTIR microscope. X-ray photoelectron spectroscopy (XPS) analysis was performed with a VG Scientific ESCALAB MK II spectrometer (UK) equipped with a Mg Kα excitation source (1253.6 eV) and a five-channeltron detection system to analyze the elemental state. Raman spectra were obtained with a Renishaw Raman microscope, equipped with a He−Ne laser excitation source emitting at a wavelength of 632.8 nm, and a Peltier cooled (−70 °C) charge coupled device (CCD) camera. Raman instrument was calibrated with silicon substrate following the routine procedure before the data acquisition. A Leica microscope with 50X objective lens was used. The holographic grating with 1800 grooves/mm and the 1 cm^{-1} slit enabled the spectral resolution. Laser power at the sample was 4.5 mW, and the data acquisition time was 30 s. UV−visible absorption spectra were recorded with a SPECTRASCAN UV 2600 digital spectrophotometer (Chemito, India).

Synthesis of Ag-rGO. Graphene oxide (GO) was chemically synthesized by the Hummers method.[40] In short, pristine graphite was oxidized by some strong oxidants such as $KMnO_4$, $NaNO_3$, conc. H_2SO_4 followed by H_2O_2 treatment to remove the excess $KMnO_4$ and synthesized MnO_2 by converting them into water-soluble $MnSO_4$. The required Ag-rGO was synthesized as follows; first 5 mg of dried GO was sonicated in 10 mL of DMF for 1 h in a beaker. In a separate beaker, 0.5 mmol $AgNO_3$ and 0.1 g of PVP were stirred in 10 mL of DMF for 1 h which resulted in the formation of Ag NPs. Then two mixtures were taken in a screw-capped test tube and heated on a water bath for 20 h. This treatment resulted in the formation of a black product which was centrifuged repeatedly at 4500 rpm with distilled water to remove the unbound Ag NPs. Finally the product (Ag-rGO) was washed with ethanol and dried under vacuum and used for further characterizations and SERS study.

Preparation of Samples for Surface Enhanced Raman Scattering (SERS). For SERS measurement, solutions of uranyl acetate (UAc) with variable concentration ranging from 10^{-3} to 10^{-8} M were prepared from 5×10^{-3} M stock solution of UAc with proper dilution with water. Into 1 mL of these solutions, 50 μL of Ag-rGO dispersion (1 mg/mL in ethanol) was added and left for 4 h of incubation. SERS spectra were recorded after dispensing the incubated sample directly onto an aluminum foil. The same procedure was also followed for other cases.

RESULTS AND DISCUSSION

A simple wet-chemical approach has been employed for the fabrication of silver nanoparticles decorated rGO nanosheets in DMF medium where DMF plays the dual role of solvent and

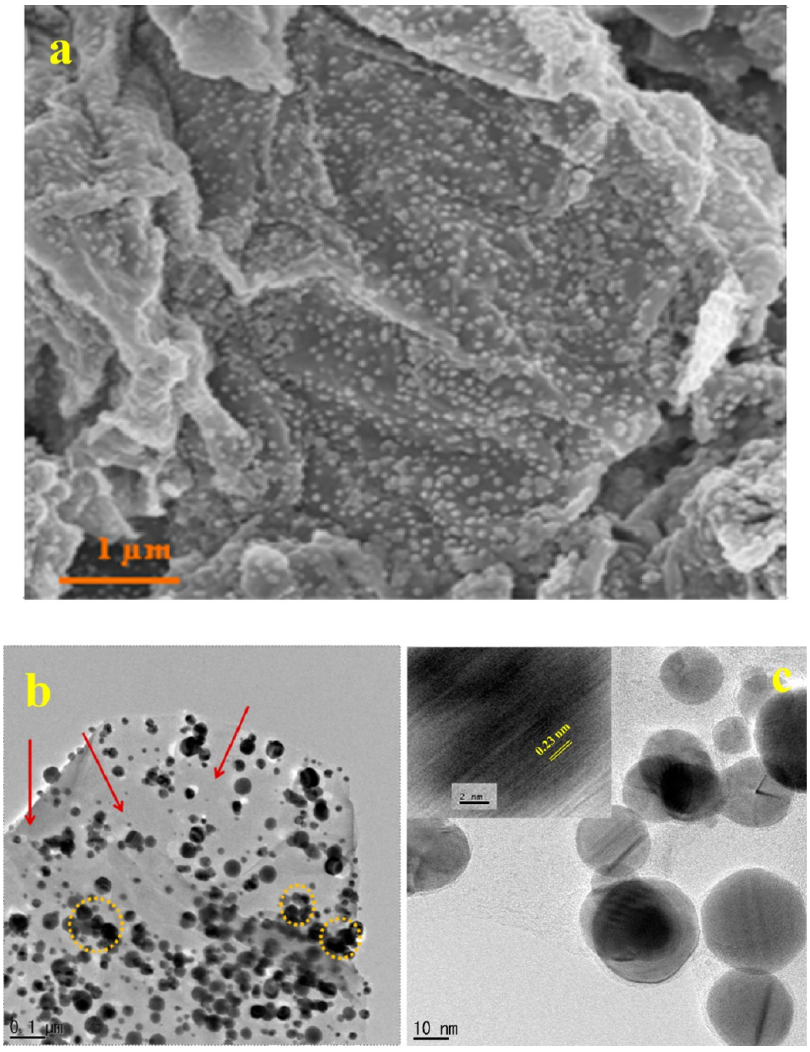

Figure 1. (a) FESEM image and (b, c) TEM images of Ag-rGO. Inset shows HRTEM image of Ag-rGO.

reducing agent. DMF can reduce GO in a microwave (MW)-assisted pathway.[41] Herein a coreduction method has been adopted for both GO and $AgNO_3$ reduction by DMF at ∼85 °C on a water bath where PVP acts as a growth controlling agent. This material (Ag-rGO) is used as a SERS substrate.

Decoration of reduced graphene oxide (rGO) sheets by silver nanoparticles (Ag NPs) was first examined with respect to the amount of silver nitrate keeping other conditions unaltered. Varying the amount of silver nitrate, we have determined that 0.5 mmol of silver nitrate is the optimized quantity for fairly uniform distribution of Ag NPs on rGO sheets (Figure S1, Supporting Information). The FESEM image in Figure 1a indicates the high density population of the Ag NPs on rGO surface. The close packed distribution of the Ag NPs over the rGO nanosheet (indicated by red arrow) is also visible from the corresponding TEM image (Figure 1b). Eventually, the nanoparticles remain closely associated with each other in some places as indicated in Figure S2. These associations could be rationalized as the "hot-spots",[42] the most desired sites to probe SERS enhancement. The nanoparticles are spherical and have an average particle size of 20−40 nm as revealed from Figure 1c. The lattice-fringe spacing from HETEM study is measured to be 0.23 nm which corresponds to the (111) crystal plane of silver crystallite as indicated in the inset of Figure 1c.

To investigate about the homogeneity of the as-synthesized sample, we have performed selected area mapping analysis which clearly reveals that synthesized Ag NPs are exclusively distributed over the whole reduced graphene oxide sheets (Figure 2). Unlike MW heating,[41] the proposed method is gifted with immobilization of aggregated bigger (20−40 nm) Ag particles in rGO matrix. Further energy-dispersive X-ray (EDX) examination during TEM analysis in Figure S3 confirms the presence of atomic silver, whereas the other elements appear due to rGO sheets and copper grid.

Figure 3a compares the powder X-ray diffraction pattern of dried GO and Ag-rGO composite. GO shows a sharp peak at around $2\theta = 9.85°$, which corresponds to d-spacing of 8.97 Å for (001) plane. This d-spacing value is much higher than graphite ($2\theta = 26.5°$; d-spacing = 3.36 Å) for (002) plane which indicates the extensive oxidation of graphite. The as-synthesized Ag-rGO material shows four intense peaks at 2θ = 38°, 44.3°, 64.45°, and 77.3°, which are assigned for (111), (200), (220), and (311) planes of Ag (JCPDS No. 04-0783). This confirms the presence of Ag NPs in face-centered cubic (fcc) phase. The sharp peak present in GO is absent in Ag-rGO, and a broad peak appears in the range of $2\theta = 20−30°$ which is assigned as the diffraction from (002) plane of the restored graphitic moiety. Here d-spacing value is 3.86 Å which

dx.doi.org/10.1021/am4025017 | ACS Appl. Mater. Interfaces 2013, 5, 8724−8732

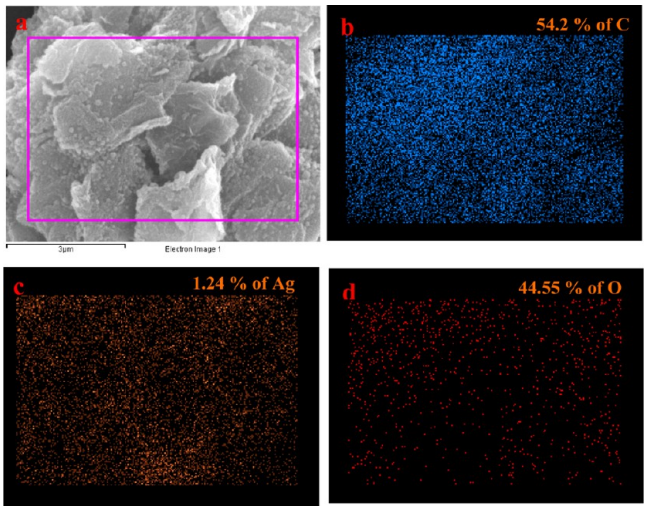

Figure 2. Area mapping analysis for each elements present in Ag-rGO. Inset shows their content in atomic percentage.

is close to the value for pristine graphite confirming the reduction of GO. Extent of GO reduction by DMF has been again investigated by FTIR spectroscopy in Figure 3b. GO exhibits a broad peak at 3410 cm^{-1} which is assigned as O−H stretching mode. The other peaks at 1719, 1395, 1217, and 1051 cm^{-1} appear due to C═O stretching mode, O−H bending mode, C−O (epoxy) stretching mode, and C−O (alkoxy) stretching mode, respectively.[43] Unoxidized sp^2 graphitic domains give signature at 1619 cm^{-1} in FTIR spectra.[43] Ag-rGO shows a decrease in intensity of the above oxygen related functional groups especially C═O and O−H groups and also arising of one new peak at 1578 cm^{-1} (skeletal C═C vibration in rGO sheets) which implies the reduction of GO.[44] Here it is worth noting that three peaks corresponding to oxygen functionalities are still present in 1400−1000 cm^{-1} wavenumber range though their intensities are reduced.

Elemental composition and also their chemical state of the graphitic materials have been examined by X-ray photoelectron spectroscopy (XPS). Figure 4a presents the C 1s XPS spectra of GO, which is evidence of three major contributing components as indexed due to sp^2 and sp^3 C (285 eV), C−O (286.6 eV) and C═O (288 eV) groups.[45] In C 1s XPS spectra of Ag-rGO (Figure 4b), the most intense peak is found to be for sp^2 C (284.6 eV) and the integrated area for sp^2 C increases along with the decrease in integrated areas for oxygenated carbon moiety as tabulated in Table S4. This observation suggests the deoxygenation of GO on reduction with DMF at 85 °C. On the other hand, Figure 4c presents the signature of Ag 3d doublet for Ag NPs where two bands at 368.6 and 374.6 eV are ascribed to the binding energies of Ag $3d_{5/2}$ and Ag $3d_{3/2}$ electronic states, respectively. These values are quite higher than those of metallic silver (0) where two bands appear at 367.9 and 373.9 eV.[46] These shifts to higher binding energy (0.7 eV) can be explained by the electron transfer from silver to graphene in Ag-rGO as the work function of silver (4.2 eV) is lower than reduced graphene oxide (rGO) (>4.8 eV depending on the amount of oxygen functionalities).[47] Again the difference between the doublets of Ag 3d electronic state is 6.0 eV which suggests the presence of Ag^0 in Ag-rGO material.[48]

Figure 5a shows the comparative Raman spectra of GO and Ag-rGO where two characteristic peaks are present. G band near 1590 cm^{-1} arises due to first order scattering of E_{2g} phonons and D band near 1330 cm^{-1} comes from the breathing mode of k-point photons of A_{1g} symmetry. Here sp^2 hybridized carbon domains are responsible for the G band, and lattice disorder is signified by the D band.[49] The intensity ratio of the above indicated two bands, that is, I_D/I_G, is the well-known signature for GO reduction. Here I_D/I_G value increases from 0.94 to 1.08 during GO to Ag-rGO conversion which indicates the formation of new and isolated smaller graphitic domains.[6] Figure 5b represents the UV−vis absorption spectra of Ag NPs (Creighton sol[50]), aqueous dispersion of GO, and resulting Ag-rGO. Two maxima from GO can be explained in terms of $\pi-\pi^*$ transition (~234 nm) and $n-\pi^*$ transition (~291 nm).[22] The main absorption peak in GO is red-shifted to 254 nm in Ag-rGO which confirms the restoration of conjugation during reduction. Another new broad peak at ~411 nm is due to the presence of plasmonic silver nanoparticles on the rGO matrix. From the above discussion, it is again concluded that GO has been partially reduced to rGO by DMF at 85 °C for 20 h of heating in water bath. Here PVP act as a stabilizer for the as-synthesized silver nanoparticles which are decorated on the sheets of reduced graphene oxide. PVP can also be a reducing agent in this case as its reducing power has been reported elsewhere.[22,51] However, its performance as stabilizer is of main importance here.[52]

SERS Study. Uranium(VI) exists as dioxouranium cation (UO_2^{2+}) which is also known as the uranyl ion, and its chemistry in aqueous solution is very complicated. Analysis and quantification of uranyl ion through SERS measurement

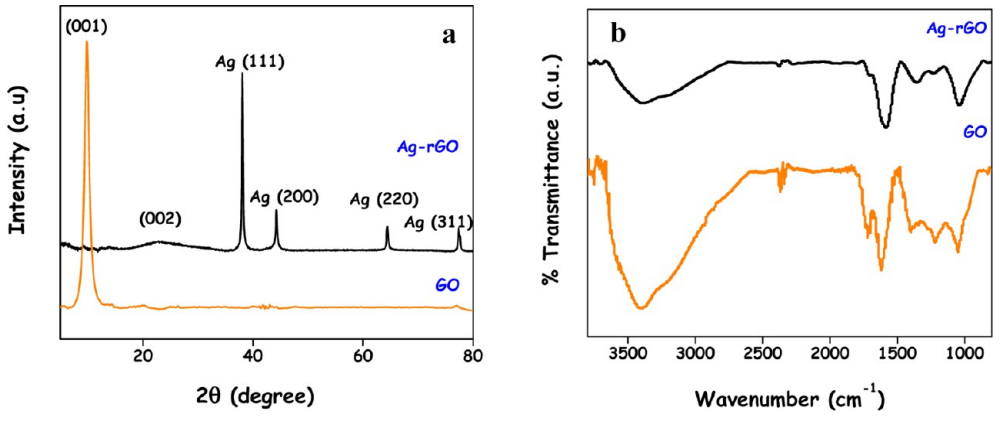

Figure 3. Comparative (a) XRD pattern and (b) FTIR spectra of GO and Ag-rGO.

dx.doi.org/10.1021/am4025017 | ACS Appl. Mater. Interfaces 2013, 5, 8724−8732

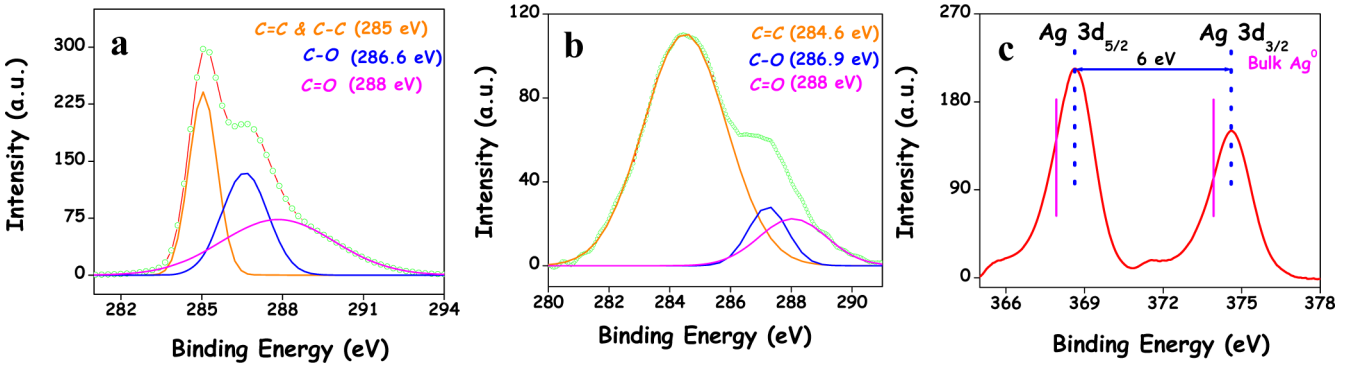

Figure 4. XPS spectra of (a) C 1s from GO, (b) C1s from Ag-rGO, and (c) Ag 3d from Ag-rGO.

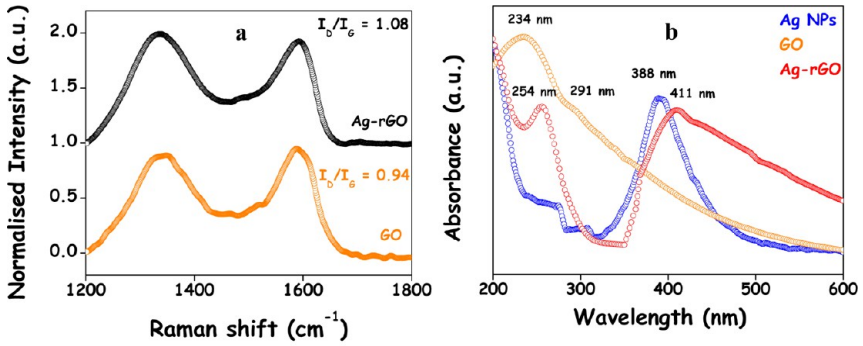

Figure 5. (a) Comparative Raman spectra of GO and Ag-rGO and (b) absorbance spectra of Ag NPs (Creighton sol), GO, and Ag-rGO.

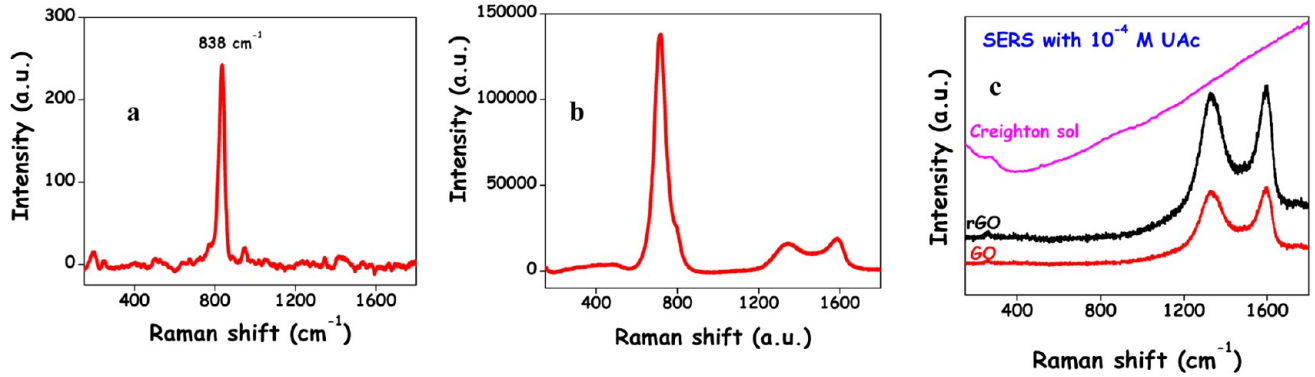

Figure 6. (a) NRS spectra of uranyl acetate (UAc) of 5×10^{-3} M aqueous solution. (b) SERS spectra on Ag-rGO with 10^{-5} M UAc. (c) SERS spectra of 10^{-4} M UAc with various substrates.

demands its high adsorption affinity and also good interactions with the substrate. Herein, reduced graphene oxide being a good adsorbent is employed as an effective platform in conjunction with Ag NPs for significant Raman enhancement of uranyl ion. Incubation time has been determined from the adsorption kinetics study of UAc by Ag-rGO substrate. Figure S6 indicates the saturated adsorption on SERS substrate after 4 h of incubation. The NRS spectrum of UAc is shown in Figure 6a where band at 838 cm^{-1} is assigned as O═U═O symmetric stretching frequency of uranyl ion. This band shifts to lower frequency at 714 cm^{-1} (with 10^{-5} M aqueous UAc solution) while the ion remains associated with the Ag-rGO substrate (Figure 6b). The estimated apparent enhancement factors (AEFs) of the symmetric stretching Raman band at 714 cm^{-1} in SERS spectra can be calculated using following relation:[53]

$$\mathrm{AEF} = I_{\mathrm{SERS}}[C_{\mathrm{NRS}}]/I_{\mathrm{NRS}}[C_{\mathrm{SERS}}] \quad (1)$$

where C and I represent the corresponding concentration of the probe molecule and the peak intensity of the Raman bands measured from baseline at respective conditions.

The AEF value is calculated to be 3×10^5 for 10^{-5} M UAc with Ag-rGO substrate. Upon increasing the amount of $AgNO_3$ (0.75 mmol instead of 0.5 mmol) during Ag-rGO synthesis, improved silver content has been observed in the substrate (Figure S7a) but it fails to exhibit better SERS activity. A comparative account has been shown in Figure S7b. Creighton sol,[50] GO, and rGO fail to show such stunning enhancement as the results are shown in Figure 6c. With Creighton sol, a large fluorescence background is observed which interferes in the SERS spectrum of UO_2^{2+} whereas in Ag-rGO fluorescence background is absent which may be due to the fluorescence quenching behavior of rGO.[13] Enhancement in the Raman signal on Ag-rGO substrate at lower concentration (10^{-5} M) is much higher compared to bare plasmonic nanoparticles (Ag

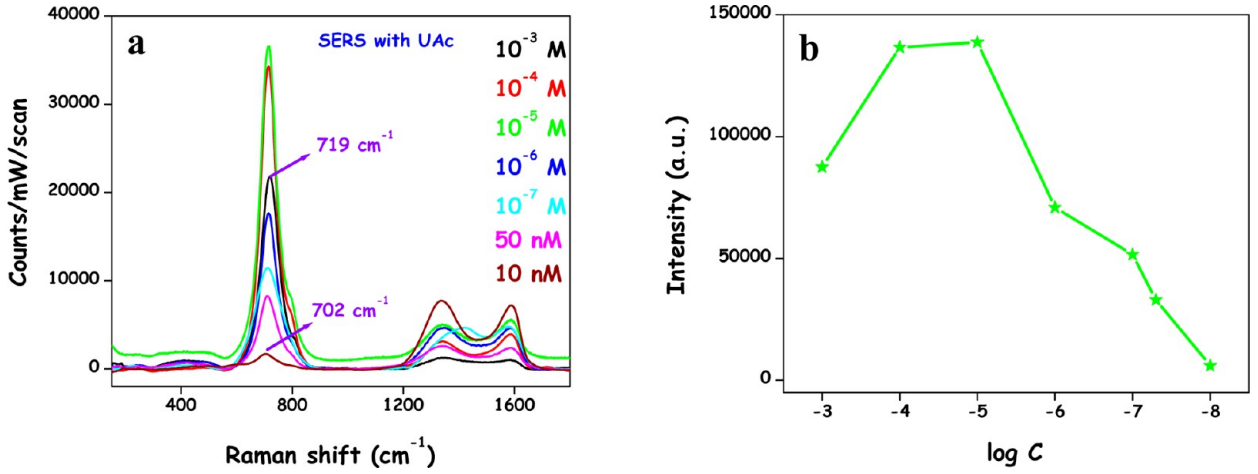

Figure 7. (a) Concentration dependent SERS spectra of UAc on Ag-rGO substrate. (b) Variation of intensity of the symmetric stretching band (centered at 710 cm^{-1}) of uranyl ion with respect to logarithm value of its concentration.

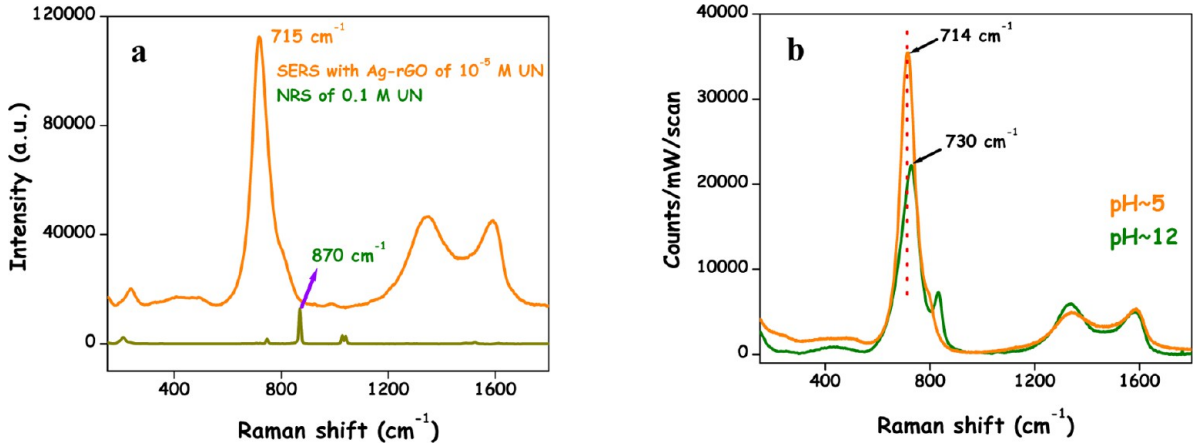

Figure 8. (a) Comparative NRS and SERS spectra of uranyl nitrate. (b) SERS spectra of 10^{-5} M aqueous UAc solution at various pH conditions.

NPs and Au NPs) as depicted in Figure S8. In Ag-rGO, extensive electronic charge transfer from silver nanoparticle to uranyl ion effectively results in weakening of the U−O bond and consequently a remarkable red shift of the uranyl Raman band (from 838 to 714 cm^{-1}) has been observed.[39] Another interesting observation has been found regarding the noticeable change in I_D/I_G ratio of Ag-rGO in the presence of uranyl species compared to its pure state where both D and G bands were distinct. But in the presence of uranyl ion, we can observe from Figure 6b that the appearance of D and G bands is not pronounced; rather these bands are quite flattened in nature (may be due to the presence of highly intense Raman band of uranyl ion). Even this nature is also evident from Figure 7a from where we can observe that the bands are distinct only when the uranyl ion concentration is in the 10 nM range and in that case it is clearly observed that the D band intensity is higher than the G band.

The enhancement of the uranyl band in Ag-rGO matrix compared to Ag NPs can be explained in terms of the aggregation of Ag NPs on reduced graphene oxide surface which in-turn introduces a large number of hot-spots. In Figure S2, several dimers or aggregates of small silver nanoparticles are located. These aggregations create hot-junctions or hot-spots where the coupled surface plasmon resonance with electromagnetic field results in highly enhanced Raman signal as addressed by different groups.[54,55] Again, the chemical effect (CE) is strongly dependent on distance between substrate and probe molecule. In the present case, reduced graphene oxide sheets play the important role of an efficient adsorbent for uranyl species through electrostatic interaction and favor the interaction between silver and uranyl ion through close proximity as found previously.[56] Though mild reduction of GO has been carried out in the experimental condition in presence of DMF and PVP, still there are some oxygen containing groups present in the Ag-rGO surface as indicated in the preceding sections, and these oxygen functionalities favor the adsorption of positively charged uranyl ions. Thus, Ag NP decorated rGO is found to be very effective for the enhancement of Raman signal where both EM and CE cojointly operate.

Figure 7a demonstrates the concentration dependent SERS spectra of UAc on Ag-rGO substrate where other parameters are kept constant. It shows that when the concentration is high (10^{-3} M), the ν_1 symmetric stretching band appears at 719 cm^{-1} and with dilution the band shifts to lower frequency. A broad band arises near 702 cm^{-1} when the concentration reaches the 10 nM level. Dilution makes a lesser number of available uranyl species for adsorption on Ag-rGO sheets. So UO_2^{2+} at lower concentration experienced more predominant charge transfer from Ag NPs compared to higher concentration resulting axial Raman band of UO_2^{2+} to shift in lower frequency. Figure 7b illustrates the variation of band intensity

dx.doi.org/10.1021/am4025017 | ACS Appl. Mater. Interfaces 2013, 5, 8724−8732

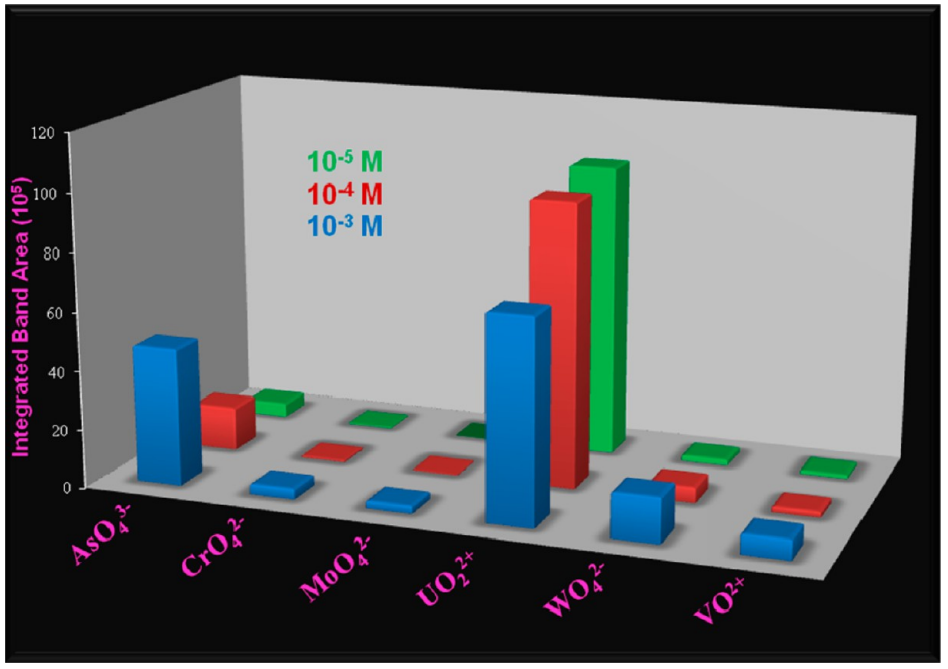

Figure 9. Diagram of integrated SERS band area vs oxo-ions at their various concentrations.

for the symmetric stretching band of uranyl with respect to logarithm of concentration of aqueous uranyl solution. It suggests that with dilution from 10^{-3} to 10^{-4}–10^{-5} M the intensity reaches its maximum, whereas sudden fall in the band intensity is observed upon dilution. The lowest band intensity has been detected in the SERS spectra when the uranyl solution is diluted to 10 nM level. This phenomenon can be explained in terms of monolayer formation[57] of the adsorbate (uranyl) on Ag-rGO substrate at 10^{-5} M concentration. At higher concentration, multilayer formation by the uranyl species (adsorbate) on the substrate prevents high enhancement of a Raman signal. Ag-rGO material shows excellent SERS enhancement when uranyl nitrate (UN) is taken in lieu of uranyl acetate (Figure 8a) where the AEF value was again calculated to be in the order of 10^5. This observation suggests the counteranion independent behavior of the observed SERS phenomenon. To test the reproducibility, SERS measurements were performed at different positions on each sample. The results are highly reproducible and the detection limit for uranyl ion is found to be 10 nM.

pH of the medium was observed to have a prominent effect on the SERS of the uranyl ion. Position of the uranyl Raman band in SERS experiment highly depends on the pH of the uranyl solution. Symmetric stretching mode of UO_2^{2+} ion is expected to exhibit variable Raman spectra especially at higher pH because of hydrolysis and hydroxyl induced polymerization of the ion. Sepaniak et al.[39] observed that the symmetric stretching mode of uranyl SERS band shifts to lower wavenumber as the UO_2^{2+} solution becomes basic. An interesting observation is put forwarded from our study; that is, the band shifts to a higher energy with increasing pH. In the SERS spectra (Figure 8b), the band around 714 cm^{-1} (pH ~ 5) shifts to 730 cm^{-1} (pH ~ 12) with 10^{-5} M UAc solution, whereas previous reports[34,39] articulated lowering of wavenumber of 30–50 cm^{-1} at respective experimental conditions. Here, it is worth mentioning that U(VI) remains as cationic UO_2^{2+} or $(UO_2)_3(OH)_5^{+}$ species at pH ~ 5 and $(UO_2)_3(OH)_8^{2-}$, an anionic moiety becomes a predominant

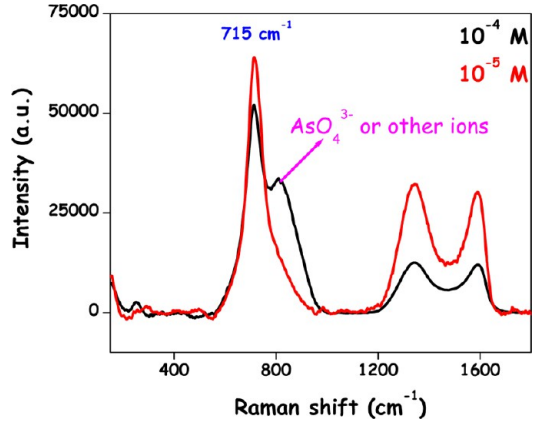

Figure 10. SERS spectra on Ag-rGO with mixed oxo-ions at two different concentrations.

species at pH ~ 12 due to hydrolysis.[39] Thus, in Ag-rGO, oxygen containing functional groups of graphitic moiety repel the negatively charged anionic U(VI) species which compel a closer association between UO_2^{2+} ion and Ag NPs as compared in Scheme 1. This creates somewhat weaker charge transfer from Ag NPs to uranyl species which results in a less significant red shifting of the symmetric stretching band of uranyl ion in SERS spectra at pH ~ 12 compared to the SERS spectra at pH ~ 5. Another interesting observation is that the Raman band of uranyl ion at pH ~ 12 appears to be broader which can be explained as the adsorption of multiple hydroxide complexes of U(VI) on Ag-rGO substrate at this experimental pH condition.

The sensitivity of the process toward uranyl ion was further supported when we performed the SERS analysis for some other common oxo-ions with the composite substrate. The various accounted ions were arsenate (AsO_4^{3-}), chromate (CrO_4^{2-}), molybdate (MoO_4^{2-}), vanadyl (VO^{2+}), and tungstate (WO_4^{2-}). SERS based detection approaches for some of these indicated oxo-ions are already reported.[58,59] In our studies, three solutions of different concentrations (10^{-3}, 10^{-4}, and 10^{-5}

dx.doi.org/10.1021/am4025017 | ACS Appl. Mater. Interfaces 2013, 5, 8724–8732

Scheme 1. Schematic Representation for the Interactions between Ag-rGO and Uranyl Species at Various pH Conditions

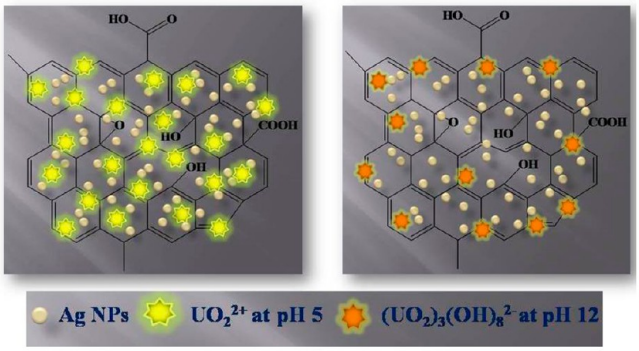

M) for each of the above-mentioned ions were used for SERS measurement, and Figure S9 shows their respective SERS spectra. In all the cases, the stretching band (ν_s) for M−O bond shifts to lower wavenumber compared to their NRS as indicated in Figure S9 (inset). Here it is worth noting that the shift in the band position is quite low for oxo-anions (AsO_4^{3-}, CrO_4^{2-}, MoO_4^{2-}, and WO_4^{2-}) whereas is higher for oxo-cations (UO_2^{2+} and VO^{2+}). This observation clearly suggests that the extent of charge transfer is insignificant for anions compared to cations and this result is quite expected. Now, the enhancement of various ions in SERS spectra can be explained in terms of strong electromagnetic effect from the aggregated Ag NPs as described earlier. The band areas for the respective band of each ion at various concentrations are also evident from Figure 9 which illustrates the highest enhancement for UO_2^{2+} ion even with 10^{-5} M leaving aside other ions. Studies on the selectivity of Ag-rGO as a SERS substrate for uranyl ion detection compared to other oxo-ions has been described in Figure 10. SERS spectra were taken for a mixed solution where all the tested oxo-ions were present at the same concentration. When the concentration is down to 10^{-5} M, it only shows the SERS signal for uranyl ion, whereas at higher concentration (i.e., 10^{-4} M) other bands also appear. This observation authenticates the high selectivity of Ag-rGO as SERS substrate toward uranyl ion, and it can be explained in terms of superior electrostatic interactions between UO_2^{2+} and Ag-rGO at lower concentration.

CONCLUSION

A simple methodology has been followed for the synthesis of silver decorated reduced graphene oxide (Ag-rGO) sheets. The as-synthesized Ag-rGO material has been employed as an efficient substrate for the first time to detect the uranyl ion (UO_2^{2+}) by surface enhanced Raman spectroscopy. Here rGO performs well and plays the following important roles: (i) facilitates the aggregation of Ag NPs which creates "hot-spot" for SERS detection and (ii) favors the adsorption of uranyl species. The red-shifting of the main featured band, that is, ν_1 symmetric stretching band, is attributed as effective CT from Ag NPs to uranyl ion. Similar results also observed with the other oxo-ions also but with band shifting and sensitivity become the main manifestation for the UO_2^{2+} ion. A detection limit of 10 nM has been achieved with this protocol. The results are highly reproducible. The substrate has been designed in a very simplified manner which creates a chance to use this potential substrate as an alternative tool for the detection of trace uranyl ion.

ASSOCIATED CONTENT

Supporting Information

FESEM images of Ag-rGO varying the amount of silver nitrate. TEM image, EDAX spectra of Ag-rGO. Table of integrated areas of various peaks present in C 1s XPS spectra for GO and Ag-rGO. Preparation of Creighton sol. UV−vis spectra of adsorption kinetics of UAc on Ag-rGO. TEM image and SERS spectra of UAc with higher $AgNO_3$ amount. SERS spectra of UAc with various substrates. SERS spectra of various oxo-ions (arsenate, chromate, molybdate, uranyl, vanadyl, tungstate) on Ag-rGO substrate. This material is available free of charge via the Internet at http://pubs.acs.org.

AUTHOR INFORMATION

Corresponding Author

*E-mail: tpal@chem.iitkgp.ernet.in.

Notes

The authors declare no competing financial interest.

ACKNOWLEDGMENTS

The authors are thankful to BRNS and CSIR, New Delhi, India, and IIT Kharagpur for financial assistance.

REFERENCES

(1) Allen, M. J.; Tung, V. C.; Kaner, R. B. *Chem. Rev.* **2010**, *110*, 132−145.
(2) Wang, X.; Zhi, L.; Mllen, K. *Nano Lett.* **2008**, *8*, 323−327.
(3) Stoller, M. D.; Park, S.; Zhu, Y.; An, J.; Ruoff, R. S. *Nano Lett.* **2008**, *8*, 3498−3502.
(4) Zhou, M.; Zhai, Y. M.; Dong, S. J. *Anal. Chem.* **2009**, *81*, 5603−5613.
(5) Kamat, P. V. *J. Phys. Chem. Lett.* **2011**, *2*, 242−251.
(6) Stankovich, S.; Dikin, A. A.; Piner, R. D.; Kohlhass, K. A.; Kleinhammes, A.; Jia, Y. Y.; Wu, Y.; Nguyen, S.; Ruoff, R. S. *Carbon* **2007**, *45*, 1558−1565.
(7) Huang, X.; Qi, X.; Boey, F.; Zhang, H. *Chem. Soc. Rev.* **2012**, *41*, 666−686.
(8) Fleischmannn, M.; Hendra, P. J.; MacQuillan, A. J. *Chem. Phys. Lett.* **1974**, *26*, 163−166.
(9) Sharma, B.; Frontiera, R.; Henry, A.; Ringe, E.; Van Duyne, R. *Mater. Today* **2012**, *15*, 16−25.
(10) Ahmed, A.; Gordon, R. *Nano Lett.* **2012**, *12*, 2625−2630.
(11) Sarkar, S.; Pradhan, M.; Sinha, A. K.; Basu, M.; Pal, T. *J. Phys. Chem. Lett.* **2010**, *1*, 439−444.
(12) Ling, X.; Xie, L. M.; Fang, Y.; Xu, H.; Zhang, H. L.; Kong, J.; Dresselhaus, M. S.; Zhang, J.; Liu, Z. F. *Nano Lett.* **2010**, *10*, 553−561.
(13) Xie, L.; Ling, X.; Fang, Y.; Zhang, J.; Liu, Z. *J. Am. Chem. Soc.* **2009**, *131*, 9890−9891.
(14) Yu, X.; Cai, H.; Zhang, W.; Li, X.; Pan, N.; Luo, Y.; Wang, X.; Hou, J. G. *ACS Nano* **2011**, *5*, 952−958.
(15) Wojcik, A.; Kamat, P. V. *ACS Nano* **2010**, *4*, 6697−6706.
(16) Wang, X.; Huang, P.; Feng, L.; He, M.; Guo, S.; Shen, G.; Cui, D. *RSC Adv.* **2012**, *2*, 3816−3822.
(17) Goncalves, G.; Marques, P. A. A. P.; Granadeiro, C. M.; Nogueira, H. I. S.; Singh, M. K.; Grácio, J. *Chem. Mater.* **2009**, *21*, 4796−4802.
(18) Ng, Y. H.; Lightcap, I. V.; Goodwin, K.; Matsumura, M.; Kamat, P. V. *J. Phys. Chem. Lett.* **2010**, *1*, 2222−2227.
(19) Rycenga, M.; Camargo, P. H. C.; Li, W.; Moran, C. H.; Xia, Y. *J. Phys. Chem. Lett.* **2010**, *1*, 696−703.
(20) Tang, X.-Z.; Li, X.; Cao, Z.; Yang, J.; Wang, H.; Pu, X.; Yu, Z.-Z. *Carbon* **2013**, *59*, 93−99.

(21) Liu, X.; Cao, L.; Song, W.; Ai, K.; Lu, L. *ACS Appl. Mater. Interfaces* **2011**, *3*, 2944−2952.
(22) Zhang, Z.; Xu, F.; Yang, W.; Guo, M.; Wang, X.; Zhanga, B.; Tang, J. *Chem. Commun.* **2011**, *47*, 6440−6442.
(23) Yang, Y. K.; He, C. E.; He, W. J.; Yu, L. J.; Peng, R. G.; Xie, X. L.; Wang, X. B.; Mai, Y. W. *J. Nanopart. Res.* **2011**, *13*, 5571−5581.
(24) Fan, J.; Shi, Z.; Ge, Y.; Wang, J.; Wang, Y.; Yin, J. *J. Mater. Chem.* **2012**, *22*, 13764−13772.
(25) Ren, W.; Fang, Y.; Wang, E. *ACS Nano* **2011**, *5*, 6425−6433.
(26) Lu, G.; Li, H.; Liusman, C.; Yin, Z.; Wua, S.; Zhang, H. *Chem. Sci.* **2011**, *2*, 1817−1821.
(27) Murphy, S.; Huang, L.; Kamat, P. V. *J. Phys. Chem. C* **2013**, *117*, 4740−4747.
(28) Zhang, L.; Jiang, C.; Zhang, Z. *Nanoscale* **2013**, *5*, 3773−3779.
(29) Liu, M.; Chen, W. *Biosens. Bioelectron.* **2013**, *46*, 68−73.
(30) Clark, D. L.; Conradson, S. D.; Donohoe, R. J.; Keogh, D. W.; Morris, D. E.; Palmer, P. D.; Rogers, R. D.; Tait, C. D. *Inorg. Chem.* **1999**, *38*, 1456−1466.
(31) Eliet, V.; Bidoglio, G.; Omenetto, N.; Parma, L.; Grenthe, I. *J. Chem. Soc., Faraday Trans.* **1995**, *15*, 2275−2285.
(32) Dai, S.; Lee, Y. H.; Young, J. P. *Appl. Spectrosc.* **1996**, *50*, 536−537.
(33) Teiten, B.; Burneau, A. *J. Raman Spectrosc.* **1997**, *28*, 879−884.
(34) Tsushima, S.; Nagasaki, S.; Tanaka, S.; Suzuki, A. *J. Phys. Chem. B* **1998**, *102*, 9029−9032.
(35) Bao, L.; Mahurin, S. M.; Haire, R. G.; Dai, S. *Anal. Chem.* **2003**, *75*, 6614−6620.
(36) Ruan, C.; Luo, W.; Wang, W.; Gu, B. *Anal. Chim. Acta* **2007**, *605*, 80−86.
(37) Leverette, C. L.; Villa-Aleman, E.; Jokela, S.; Zhang, Z. Y.; Liu, Y. J.; Zhao, Y. P.; Smith, S. A. *Vib. Spectrosc.* **2009**, *50*, 143−151.
(38) Jiang, Z.; Yao, D.; Wen, G.; Li, T.; Chen, B.; Liang, A. *Plasmonics* **2013**, *8*, 803−810.
(39) Bhandari, D.; Wells, S. M.; Retterer, S. T.; Sepaniak, M. J. *Anal. Chem.* **2009**, *81*, 8061−8067.
(40) Hummers, W. S.; Offeman, R. E. *J. Am. Chem. Soc.* **1958**, *80*, 1339.
(41) Liu, S.; Tian, J.; Wang, L.; Sun, X. *J. Nanopart. Res.* **2011**, *13*, 4539−4548.
(42) Lee, S. J.; Baik, J. M.; Moskovits, M. *Nano Lett.* **2008**, *8*, 3244−3247.
(43) Zhuo, Q.; Ma, Y.; Gao, J.; Zhang, P.; Xia, Y.; Tian, Y.; Sun, X.; Zhong, J.; Sun, X. *Inorg. Chem.* **2013**, *52*, 3141−3147.
(44) Nethravathi, C.; Rajamathi, M. *Carbon* **2008**, *46*, 1994−1998.
(45) He, Y.; Cui, H. *J. Mater. Chem.* **2012**, *22*, 9086−9091.
(46) Pol, V. G.; Srivastava, D. N.; Palchik, O.; Palchik, V.; Slifkin, M. A.; Weiss, A. M.; Gedanken, A. *Langmuir* **2002**, *18*, 3352−3357.
(47) Wu, T.; Shen, H.; Sun, L.; Cheng, B.; Liu, B.; Shen, J. *ACS Appl. Mater. Interfaces* **2012**, *4*, 2041−2047.
(48) Ma, J.; Zhang, J.; Xiong, Z.; Yong, Y.; Zhao, X. S. *J. Mater. Chem.* **2011**, *21*, 3350−3352.
(49) Ferrari, A. C.; Robertson, J. *Phys. Rev. B* **2000**, *61*, 14095−14107.
(50) Creighton, J. A.; Blatchford, C. G.; Albrecht, M. G. *J. Chem. Soc., Faraday Trans. 2* **1979**, *75*, 790−798.
(51) Weng, G.; Mahmoud, M. A.; El-Sayed, M. A. *J. Phys. Chem. C* **2012**, *116*, 24171−24176.
(52) Tang, X.-Z.; Cao, Z.; Zhang, H.-B.; Liu, J.; Yu, Z.-Z. *Chem. Commun.* **2011**, *47*, 3084−3086.
(53) Sarkar, S.; Pande, S.; Jana, S.; Sinha, A. K.; Pradhan, M.; Basu, M.; Chowdhury, J.; Pal, T. *J. Phys. Chem. C* **2008**, *112*, 17862−17876.
(54) Lee, S. J.; Morrill, A. R.; Moskovits, M. *J. Am. Chem. Soc.* **2006**, *128*, 2200−2201.
(55) Li, W.; Camargo, P. H. C.; Lu, X.; Xia, Y. *Nano Lett.* **2009**, *9*, 485−490.
(56) Yan, W.; Bao, L.; Mahurin, S. M.; Dai, S. *Appl. Spectrosc.* **2004**, *58*, 18−25.
(57) Chowdhury, J.; Ghosh, M. *J. Colloid Interface Sci.* **2004**, *277*, 121−127.
(58) Mulvihill, M.; Tao, A.; Benjauthrit, K.; Arnold, J.; Yang, P. *Angew. Chem., Int. Ed.* **2008**, *47*, 6456−6460.
(59) Mosier-Boss, P. A.; Lieberman, S. H. *Appl. Spectrosc.* **2003**, *57*, 1129−1137.